RELATIONSHIP BETWEEN SOIL MOVEMENT AND POWER CONSUMPTION IN A FURROW-OPENING ROTARY BLADE
/
圆盘式开沟刀土壤移动规律与功耗关系研究

Kuan Qin, Xiaolong Liang, Chengmao Cao*), Liangfei Fang
College of Engineering, Anhui Agricultural University, Anhui Province, Hefei 230036, China
Corresponding author, Tel: +8615205111399; E-mail address: caochengmao@sina.com
First author , Tel: +8618855102551; E-mail address: qinkuan@ahau.edu.cn
DOI: https://doi.org/10.35633/inmateh-62-06

Keywords: *rotary blade, tracer method, soil movement, movement distance, power consumption*

ABSTRACT

Small, handheld furrow openers using rotary blades usually have limited power, making it necessary to minimise their operating power consumption, which mainly occurs with the soil throwing and movement of rotary blades. To this end, it is necessary to investigate the power consumption of such tillage implements, particularly the relationship between their power consumption and operating conditions based on soil movement patterns. In this study, we performed a field test of a furrow-opening rotary blade using round, physical tracers to monitor soil movement. The total power consumption of the rotary blade was positively related to the operating depth of the blade but was not related to the soil movement distance. The total power consumption peaked at 6.677 kW at a forward speed of 0.3 m/s, which was negatively related to the forward speed, but positively related to the soil movement distance. At a blade rotational speed of 340 rpm, the total power consumption peaked at 4.385 kW and was positively related to the blade rotational speed and soil movement distance. Therefore, it was concluded that by decreasing the rotary blade rotational speed and operating depth and increasing the forward speed, the power consumption of the unit working length can be reduced.

摘要

小型手扶式开沟机对所使用的旋转式开沟刀具有动力限制，因此需要减小开沟刀作业过程中抛撒与移动土壤的阻力，为了达到减小作业阻力的目的，对开沟刀作业过程中的土壤移动规律与开沟功耗进行研究。通过圆形示踪颗粒代替土壤，通过追踪示踪颗粒达到测定土壤移动规律的目的，再此过程中同时测定作业功耗，得到土壤移动规律与旋转式开沟刀作业功耗之间关系。通过试验可知，开沟刀作业功耗和开工深度呈正相关，与土壤移动距离无关。开沟刀在作业速度 0.3 m/s 时，作业功耗最大为 6.677 kW；开沟刀在作业速度 340 rpm 时，作业功耗最大为 6.677 kW。通过试验结果可知，当减小开沟刀旋转速度和开沟深度，增加开沟刀前进速度时，可使单位工作距离下，旋转式开沟刀作业阻力最小。

INTRODUCTION

Small, handheld furrow openers are widely used for preparing small field patches, particularly those in hilly and mountainous regions, owing to their better manoeuvrability in small spaces, lower power consumption, and greater slope-climbing capability as compared with large furrow openers. These furrow openers usually use disc-type rotary blades fixed to a rotating shaft (Figure 1a). To reduce the power consumption of such furrow openers, the resistance force on their rotary blades needs to be minimised (*Matin et al., 2015*), making it necessary to investigate the occurrence mechanism of the resistance. The resistance on rotary blades is the reacting force of their soil-cutting force (*Kataoka et al., 2002; Ani et al., 2018*). The occurrence mechanism of the resistance has been investigated using various methods. *Li et al. (2018)* investigated the occurrence mechanism of the resistance on rotary blades using smoothed particle hydrodynamics and Taguchi methods. *Asl et al. (2009)* developed a mathematical model for predicting the power requirement of rotary blades and equations for quantifying blade surface area per unit volume of soil tilled, thereby optimising blade structure for resistance minimisation. *Salokhe et al. (2002)* experimentally investigated the resistance on reverse and traditional rotary blades operating at different rotational speeds in clay soil. *Yang et al. (2015)* developed a soil-cutting model of rotary blades using a finite element method, observing that the power consumed during soil cutting mainly consisted of kinetic and internal power, with a ratio of kinetic power to internal power of 1:9.5. *Chertkiattipol et al. (2010)* investigated the resistance on rotary blades at different temporal phases by measuring their coordinates at various time points. In addition,

past research into the effect of the structure of rotary blades on their cutting force has also been investigated *(Ahmadi et al., 2017; Fajardo et al., 2014; Mollazade et al., 2009)*. Furrow opening using rotary blades involves moving soil outside of the furrow *(Lee et al., 2003)*, with the kinetic and potential energies required for moving soil provided by the rotary blades. Thus, soil movement patterns affect the energy consumption of rotary blades *(Shibusawa, 1993). Ucgul et al. (2017; 2018b)* investigated the soil movement and tillage force of a mouldboard plough and rotary spader through discrete element modelling. *Li et al. (2019)* marked soil layers using physical tracers and analysed soil movement using a digital image processing technique. *Haas et al. (2018)* measured soil movement using different corpuscular metal tracers and a metal detector. *Grayling et al. (2018)* traced particle movement in soil using X-ray micro computed tomography. *He et al. (2016)* investigated the penetration force of a shovel-type furrow opener using a finite element method. The soil movement and cutting force of various tillage implements have been investigated. Traction-type implements involve only *in-situ* soil movement *(Qin et al., 2018)*. In contrast, furrow-opening rotary blades involve soil cutting, crushing, and throwing *(Harrison, 1978)*. This process involves both short- and long-distance movement of scattering soil (Figure 1b), thereby moving soil from inside the furrow to targeted positions outside of the furrow. The power consumption of this process constitutes the majority of the power consumed by the furrow-opener. Thus, the soil movement patterns are key to the occurrence mechanism of the resistance on rotary blades.

In this study, the relationship between furrow-opening rotary blades and operating conditions was investigated based on soil movement pattern, and an optimal level of energy consumption of the furrow-opening rotary blade under different operating conditions was determined.

Physical tracers are most appropriate for tracing the soil movement and throwing operations of furrow-opening rotary blades. However, tracers used in previous experiments were large, heavy, and mostly polyhedral, features which are not appropriate for tracing the soil movement and throwing of furrow-opening rotary blades *(Rahman et al., 2005; Viktor et al., 2018; Solhjou et al., 2012)*. In this study, a small-diameter round tracer similar to a soil pellet was used to investigate the soil throwing and movement produced by furrow-opening rotary blades, and their power consumption was investigated in relation to the operating conditions and soil movement pattern.

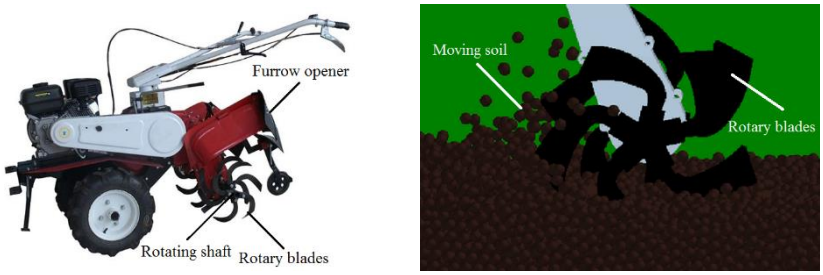

(a) *(b)*

Fig. 1 - Furrow-opening rotary blade

(a) Small handheld furrow-opening rotary blades and soil movement during operation; (b) Soil throwing and movement of furrow opening rotary blades

MATERIALS AND METHODS

Field test platform

A field test platform was established to measure the soil movement and cutting force of furrow-opening rotary blades when the rotary blades were operating (Figure 2). The platform consisted of a frame, 48-V power source, forward drive motor, motor speed controller, gasoline engine, gear box, chain drive for driving the rotary blades, shaft for mounting the disc blades, torque sensor, computer, furrow-depth adjustment unit, traction wheels, and depth roller. The power source provided power to the driving motor, which drove the traction wheel to move forward. The forward movement speed of the platform was adjusted through the motor speed controller. The gasoline engine drove the shaft (on which the discs blades were mounted) through the gear box and chain drive. The output speed of the gear box could be adjusted to four different levels. The shaft rotated at high speeds to drive the furrow-opening rotary blades. The torque sensor was fixed to a position between the gasoline engine and shaft for measuring in real-time the rotational speed and power consumption (torque and power, respectively) of the rotary blades; torque and power measurements were collected every second. Measurements were inputted into the computer through a wireless transmitter and were displayed on the computer screen. The data acquisition software (Labview) collected torque and power measurements according to the current frequency, and automatically output the total power

consumption for a given period. The soil cutting depth of the rotary blades was adjusted by modifying the distance between the frame and depth roller through the operating depth adjustment unit.

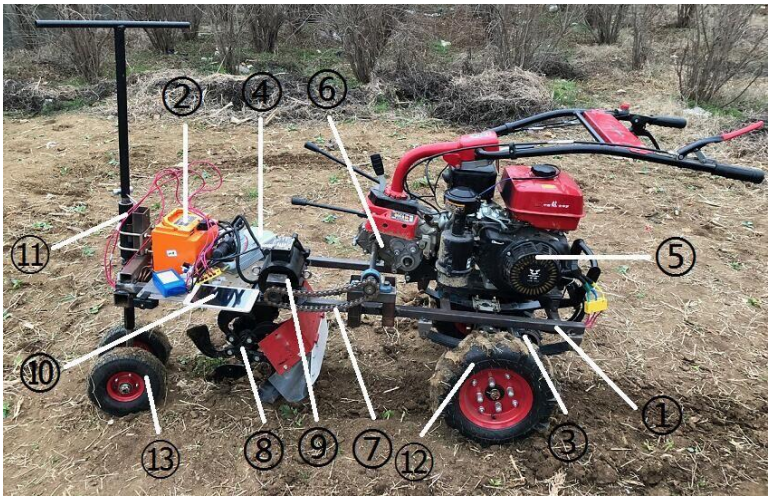

Fig. 2 - Field test platform

1 - Frame; 2 - Power source; 3 - Forward drive motor; 4 - Motor speed controller; 5 - Gasoline engine; 6 - Gear box; 7 - Chain drive; 8 - Shaft for mounting blade discs; 9 - Torque sensor; 10 – Computer; 11 - Operating depth adjustment unit; 12 - Traction wheel; 13 - Depth roller

Rotary blade

The rotary blade used for the test had lateral and forward cutting edges (Fig. 3a). The cutting edges were in different spatial planes, with the lateral cutting edge represented using coordinate system *oxyz* and the forward cutting edge represented using coordinate system $o_b x_b y_b z_b$. The radius of gyration of the rotary blade, *R*, measured 260 mm. The lateral and forward cutting edges were in-plane isometric spirals. The lateral cutting edge was represented in plane coordinate system *oxyz* and can be described using Eq. (1):

$$\rho = 168 + 3.7\theta \quad (1)$$

where: θ represents the polar angle of the spiral, with the polar angle at the starting point of the spiral $\theta_0 = 0°$ and at the ending point $\theta_n = 22.3°$; and ρ is the polar radius of the spiral, with the polar radius at the starting point of the spiral $\rho_0 = 168$ mm and at the ending point $\rho_n = 250$ mm.

The plane of the forward cutting edge deflected around line *l* at an angle of $\psi = 74°$, with the angle between line *l* and x-axis $\beta = 58°$. The forward cutting edge was represented in plane coordinate system $o_b x_b y_b$ and can be described using Eq. 2:

$$r = 214 + 3.2\delta \quad (2)$$

where: δ is the polar angle of the spiral, with the polar angle at the starting point of the spiral $\delta_0 = 0°$ and at the ending point $\delta_n = 12.6°$; and *r* is the polar radius of the spiral, with the polar radius at the starting point of the spiral $r_0 = 184$ mm and at the ending point $r_n = 212$ mm.

The widths at the root, deflection, and tip of the blade, h_1, h_2, and h_3, measured 32, 47, and 56 mm, respectively. Five blades were arranged circumferentially at an equal angular distance to form a disc (Figure 3b). The radius of gyration of the disc measured 300 mm. The blades were made using 65 Mn steel, which had a density of 7.83×10^3 kg·mm^{-3}, modulus of elasticity of 2.06×10^{11} Pa, and Poisson ratio of 0.35.

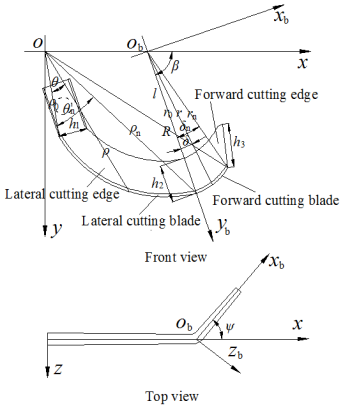

(a) *(b)*

Fig. 3 - Rotary blade

(a) Illustration of the structure of the rotary blade; (b) Rotary blade disc

Physical tracers

Small, physical tracers made from silica gel were used, each measuring 0.6 g in weight, 6 mm in diameter, 5.3 g/cm^3 in density, and an elasticity modulus of 1.2 GPa (Figure 4). Owing to similar material properties found within soils, the tracers were mixed into soils to monitor the soil movement of the furrow-opening rotary blade. Tracer pellets were numbered (1–30), and their movement was used to represent soil displacement.

Fig. 4 - Tracer pellets

Methods

Configuration of tracer pellets in soil

An area of farming field measuring 5 × 1 m was randomly selected for the test. Numbered tracer pellets were then placed in the test area as follows: tracer pellets for each 5 cm soil layer (altogether five rows of tracer pellets; Fig. 5), with the distance between tracer pellets measuring 4 cm in the width direction and 100 cm in the travel direction length (four lines of tracer pellets in the width direction and six columns of tracer pellets in the travel direction; Fig. 5). To present the position of the tracer pellets, a coordinate system *XYZ* was established, with the X-, Y-, and Z-coordinates representing the travel, width, and depth directions, respectively. A total of 120 tracer pellets were used for this configuration, with each pellet representing the soil volume around it. Thus, movement of the tracer pellets represented the soil movement of the furrow-opening rotary blade.

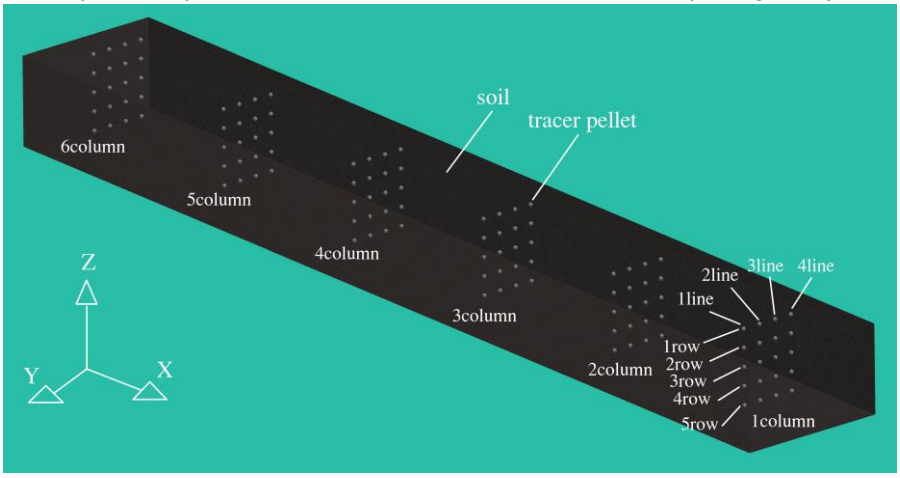

Fig. 5 - Illustration of tracer pellet configuration

Definition of test variables

The experiment was performed at the four operating depths of the furrow-opening rotary blade (5, 10, 15, and 20 cm), three forward speeds of the platform (0.3, 0.5, and 0.7 m/s), and three rotational speeds of the rotary blade (170, 255, and 340 rpm). Only one of the three variables was varied at a time. Thus, the test was performed at a total of ten levels, so that the effect of each of the variables on the soil movement and power consumption of the rotary blade was investigated. Table 1 shows the soil parameters.

Table 1

Main soil parameters of test field

Parameters	Value
Bulk density [t·m^{-3}]	1.31
Wet density [t·m^{-3}]	1.8
Soil texture	Clay loam (23.60% clay, 40.82% silt, 35.55% sand)
Dry basis soil moisture content [%]	28.98
Soil cohesion [kPa]	45.01(0-2 cm), 53.44(4-6 cm), 64.16 (8-10 cm)
Soil con index [kPa]	695(0 cm), 994(5 cm), 1207(10 cm)

Experimental procedure and data collection

Tracer pellets were buried in holes drilled in the soil according to the configuration in Figure 6(a). The rotary blade discs were fixed onto and driven by the rotating shaft of the field test platform for furrow opening (Figure 6(b)). For each level of the experiment, the platform was operated for furrow opening along the first line of tracer pellets in the width direction (because the rotary blades threw soil to the two sides symmetrically, soil movement at only one side was measured). Thus, the first line of tracer pellets was the centre of action of the rotary blade. Each level of the experiment was performed five times, with the measurements averaged for subsequent analyses. Measurements of the movement distance of the tracer pellets (Figure 6(c)), instantaneous torque (instantaneous power), and total power consumption (Figure 6(d)) were obtained from the experiment.

(a) *(b)* *(c)* *(d)*

Fig. 6 - Illustration of test procedure

(a) Tracer pellets set; (b) Platform; (c) Data measurements; (d) Power consumption collected

Methods for obtaining measurements of tracer pellet movement

Measurements of tracer pellet movement in the travel, width, and depth directions (*i*, *j*, and *z*, respectively) represented in the coordinate system defined above were obtained from the experiment and used to compute overall tracer pellet movement distance, *L*, using Equation 3:

$$L = \sqrt{i^2 + j^2 + z^2} \tag{3}$$

Methods for obtaining measurements of instantaneous torque (instantaneous power) and total power consumption

Measurements of instantaneous torque obtained by the torque sensor were collected every second and were then used to compute instantaneous power using Equation 4:

$$P = \frac{T \cdot n}{9550} \tag{4}$$

where:

P is the power (kW), T is the torque (N•m), and n is the rotational speed of the rotary blade (rpm).

At the end of each level of the test, the computer provided the output of the total power consumption for the entire length of travel (5 m) by analysing the measurement data using LabVIEW. Through the Origin8.5 software analysed the data and obtained the standard deviation of homogeneous data (error bars) and significant difference of inhomogeneous.

RESULTS AND DISCUSSION

Effect of operating depth on soil movement

When the blade rotational speed (225rpm) and forward speed (0.5m/s) were held constant, the movement distances of the first and second lines of tracer pellets were larger than those of the third and fourth lines, with the movement distance of the fourth line being the smallest. The first line was located at the centre of action of the rotary blade, the second line was close to the centre of action, and the third and fourth lines were gradually farther away from the centre of action. This indicates that the soil movement distance was the largest at the centre of action and decreased as the distance from the centre of action increased (Figure 7-10).

In Figure 7 through 10, the tracer movement distance consisting of movement in the travel, width, and depth directions is presented by the line charts, and the proportional relationship between the three components is presented by the pie charts. The proportional relationship of the three components showed that, for all soil layers at all different operating depths, the movement distance in the travel direction is larger than that in the width direction, followed by that in the depth direction. This indicates that, at all blade operating depths, the soil movement distance in the travel direction is larger than that in the width direction, followed by that in the depth direction.

Additionally, the proportion between the soil movement distances in the travel, width, and depth directions was not related directly to the operating depth. At all operating depths, the proportion of movement distance in the depth direction to the overall movement distance of deeper tracer pellets was larger than that of shallower tracer pellets. This indicates that the proportion of soil movement distance in the depth direction to the overall soil movement distance increased as the depth of the soil layer increased.

At a blade operating depth of 20 cm, for all lines of tracer pellets, the movement distance of the second row was the largest, and that of the fifth row was the smallest. As the numbering of the tracer pellet row decreased, the proportion of the tracer movement distance in the width direction in the overall tracer movement distance exhibited an increasing trend. The proportion of the movement distance in the depth direction exhibited a decreasing trend. The proportion of the movement distance in the travel direction first decreased then stabilised but was > 50% in all cases (Fig. 7). This indicates that, at a blade operating depth of 20 cm, the soil movement distance was the largest at a soil layer depth of approximately 5 cm and was the smallest at a soil layer depth of approximately 20 cm. Additionally, a deeper soil layer had a larger proportion of soil movement in the depth direction, and a shallower soil layer had a larger proportion of soil movement in the width direction.

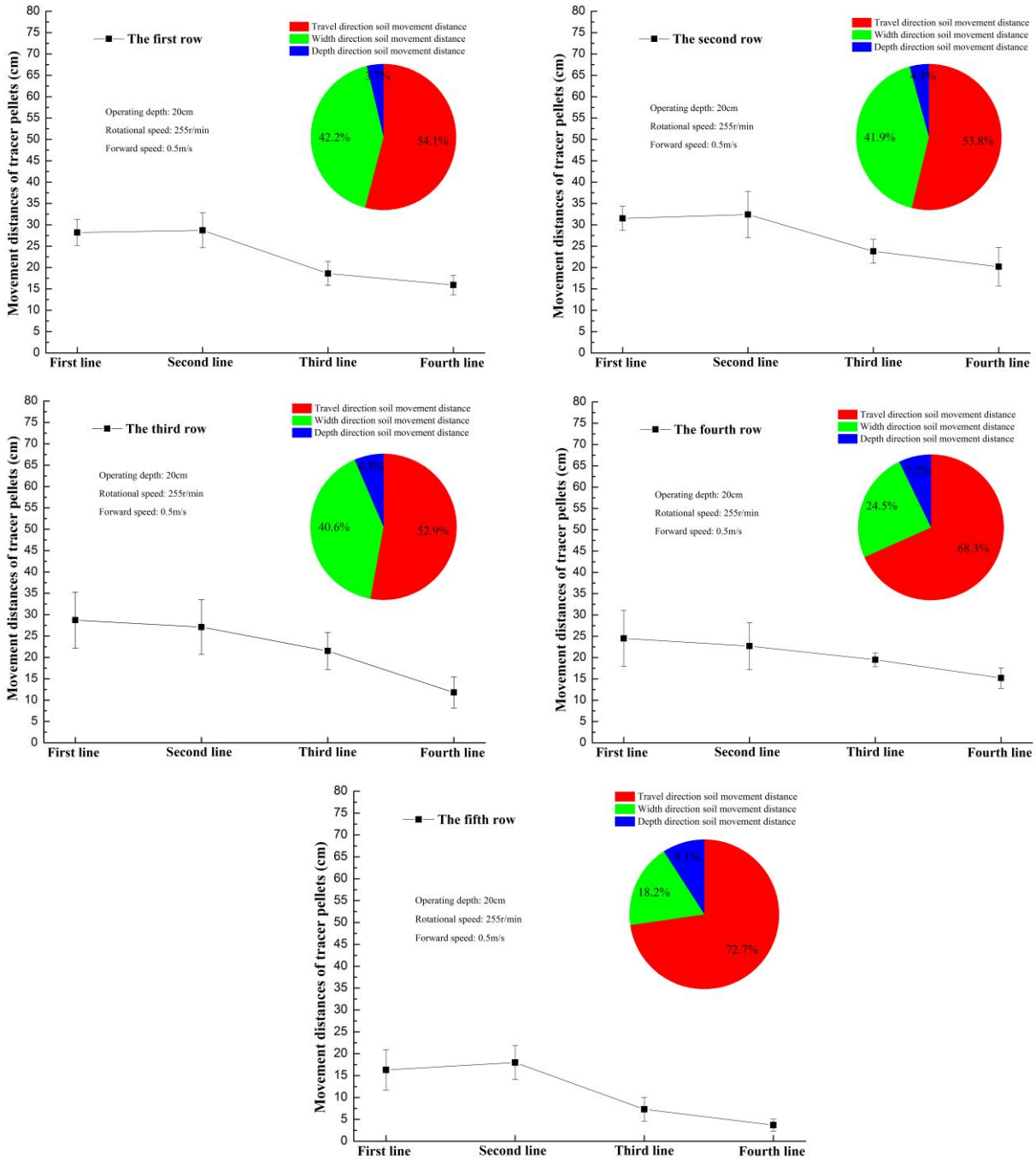

Fig. 7 - Soil movement at operating depth of 20 cm

At a blade operating depth of 15 cm, for all lines of tracer pellets, the tracer movement distance gradually decreased as the numbering of the tracer pellet row increased. Except for the fifth row, as the numbering of the tracer row decreased, the proportion of the tracer movement distance in the width direction to the overall tracer movement distance exhibited an increasing trend. The proportion of the tracer movement distance in the travel direction exhibited a decreasing trend but was > 50% in all cases (Figure 8).

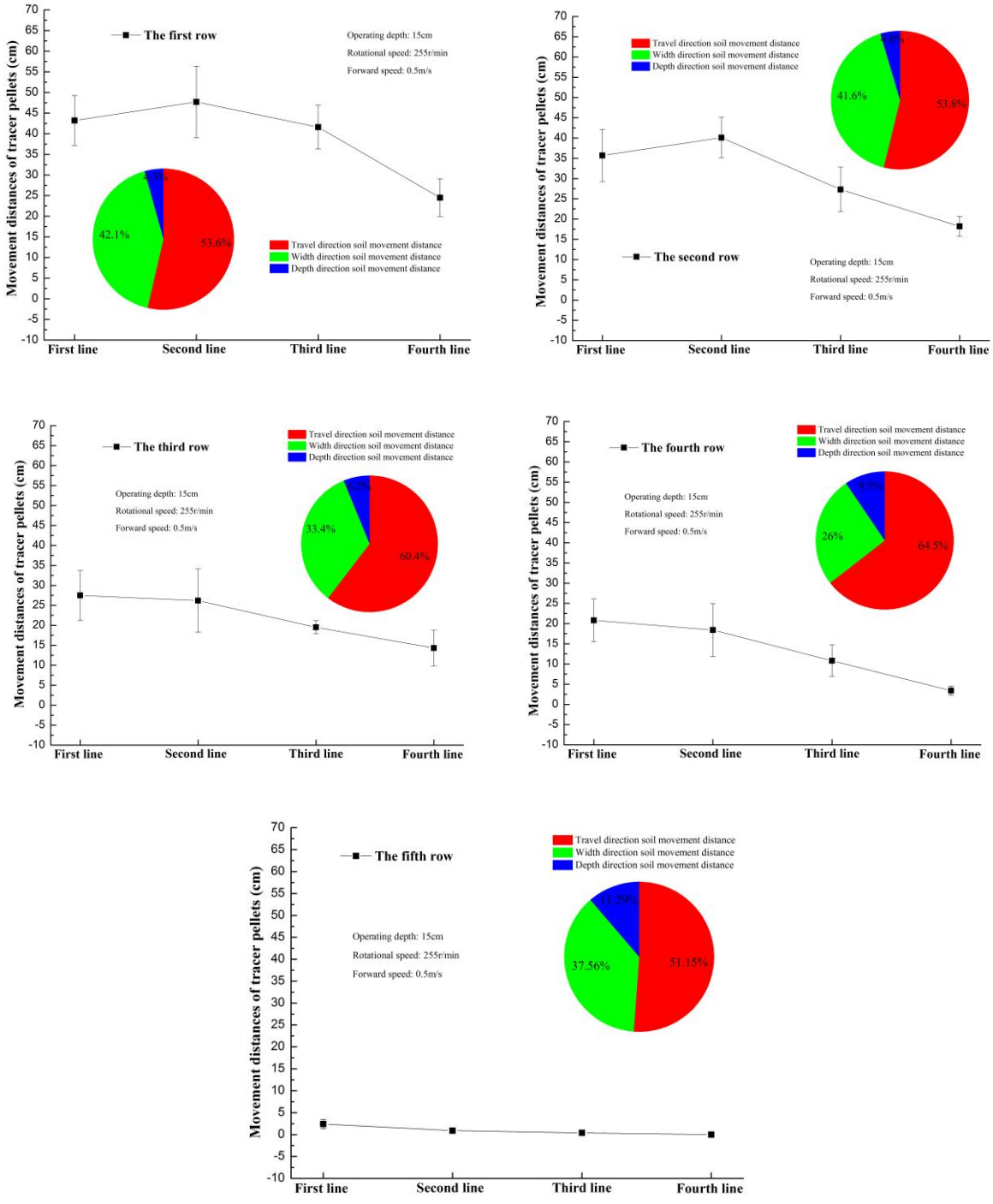

Fig. 8 - Soil movement at operating depth of 15 cm

This indicates that, at a blade operating depth of 15 cm, the soil movement distance was the largest in the surface soil layer and decreased as the soil layer depth increased. Additionally, except for the soil layer with a depth of approximately 20 cm, a shallower soil layer had a larger proportion of soil movement distance in the width direction, and a deeper soil layer had a larger proportion of soil movement distance in the travel direction.

At a blade operating depth of 10 cm, the movement distance of the tracer pellets in the second row of the second line was larger than that in the second row of the first line the difference was insignificant ($p < 0.05$).

In all other cases, the tracer movement distance was the largest in the first row and decreased as the numbering of the tracer row increased (Figure 9). This indicates that, at a blade operating depth of 10 cm, the soil movement distance was the largest in the surface soil layer and decreased as the soil layer depth increased.

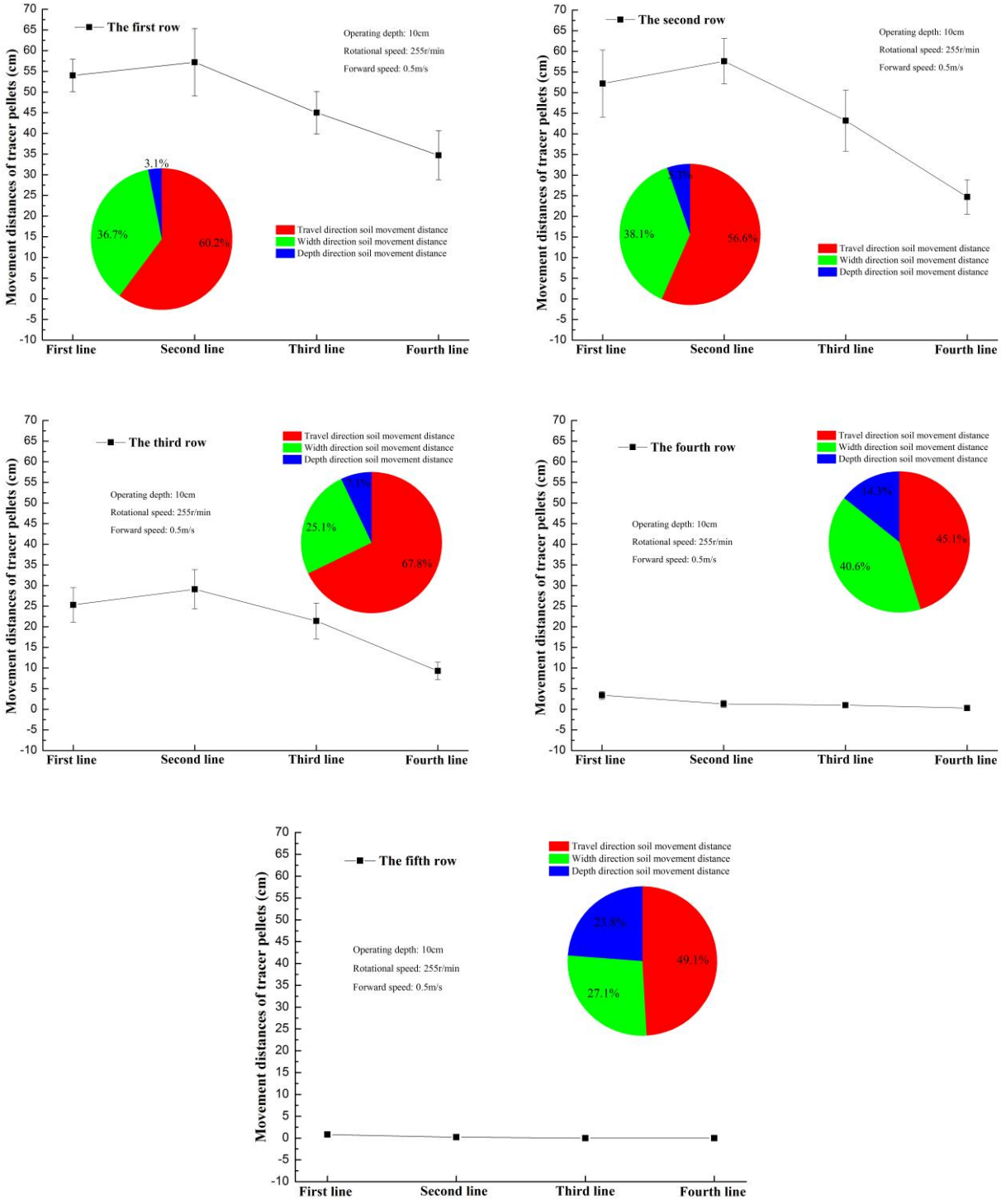

Fig. 9 - Soil movement distance at operating depth of 10 cm

At a blade operating depth of 5 cm, for all lines of tracer pellets, the tracer movement distance in the second row was the largest, followed by that in the first row; for all other rows, the tracer movement distance decreased as the numbering of the tracer row increased. In particular, the tracer pellets in the fifth row did not move (Figure 10). This indicates that, at a blade operating depth of 5 cm, the soil movement distance was the largest at a soil layer depth of approximately 5 cm, followed by that of the surface soil layer; and the soil layer with a depth of approximately 20 cm did not move.

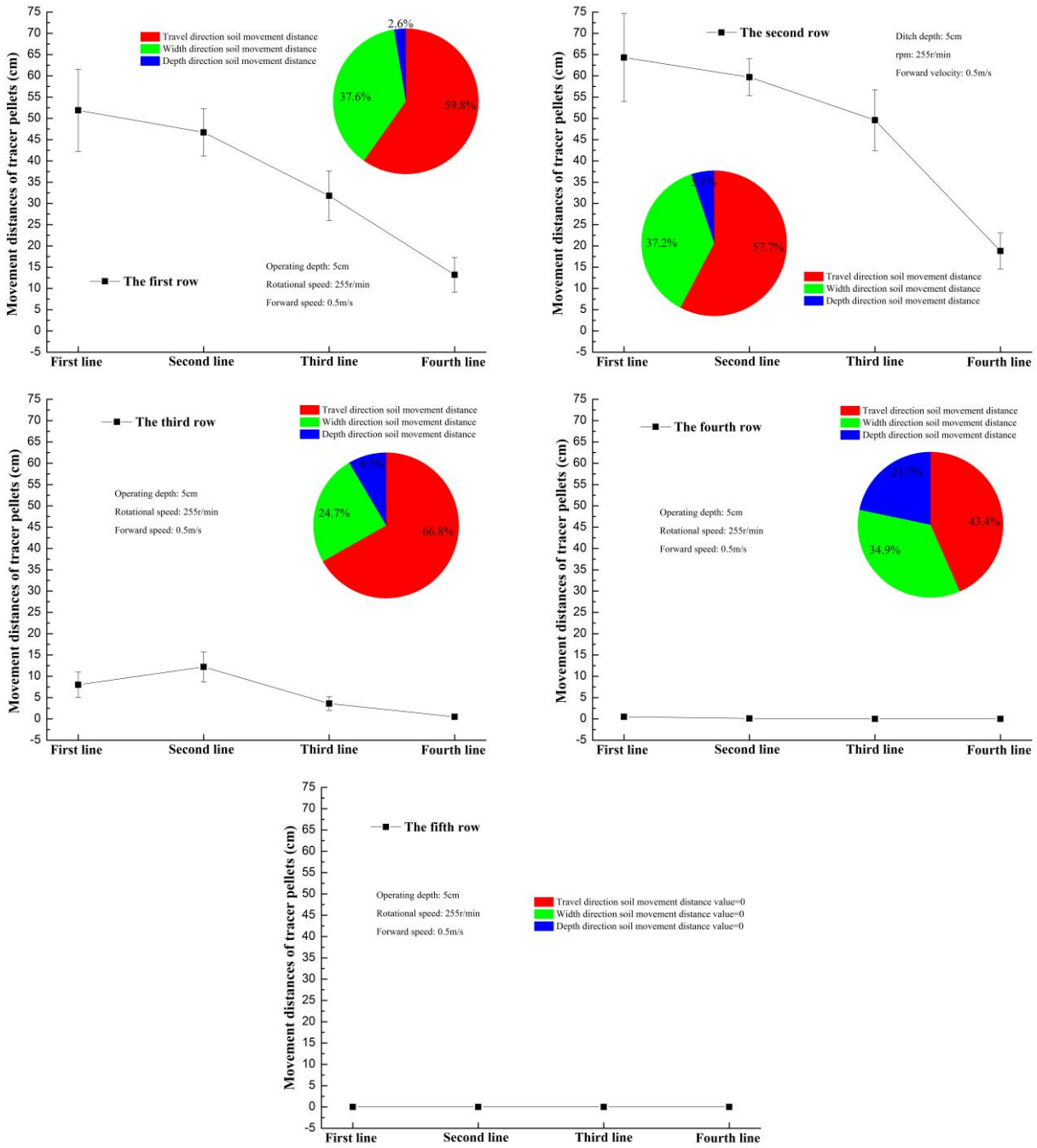

Fig. 10 - Soil movement at operating depth of 5 cm

The distance of the tracer movement by the tracer row was also analysed (Figure 7-10). The movement distance of the first row of the tracer pellet was the greatest at an operating depth of 10 cm and decreased as the operating depth increased or decreased from this level. This indicates that the soil movement distance was the greatest at an operating depth of 10 cm. At an operating depth of 5 cm, the movement distance of the first three lines in the second row of tracer pellets was the greatest, and it decreased as the operating depth increased. This indicates that the soil movement in the 5 cm depth soil layer was the greatest at an operating depth of 5 cm and decreased as the operating depth increased. At an operating depth of 20 cm, the movement distance of the third row of tracer pellets was smaller than that of the other rows, while at the other operating depths, the movement distance of the third row did not vary considerably. This indicates that the soil movement distance of the 10 cm depth soil layer did not vary considerably at operating depths of 5, 10, and 15 cm but smaller at an operating depth of 20 cm. The movement distance of the fourth and fifth rows of the tracer pellets increased as the operating depth increased. In particular, at an operating depth of 5 cm, the tracer pellets in the fifth row did not move. This indicates that the soil movement distance in the soil layers with depths of 15–20 cm was positively related to the operating depth. At an operating depth of 5 cm, the soil layers did not move.

Effect of forward speed and blade rotational speed on soil movement

Figure 11 shows the soil movement patterns at different forward speeds and blade rotational speeds. For a constant operating depth (15 cm) and blade rotational speed (255 rpm), the movement distance of the second line in the fifth row of the tracer pellets first decreased, and then increased as the forward speed increased. The movement distance of the fourth line in the fourth row peaked at a forward speed of 0.3 m/s and 0.5 m/s were equal to that at the forward speed of 0.7 m/s. The movement distance of all other rows and lines of the tracer pellets decreased as the forward speed increased (Figure 8). This indicates that soil movement distance generally increased as the forward speed decreased in the normal range. At a forward speed of 0.3 m/s, the movement distance of the second line in the second row of tracer pellets was greatest (57.9 cm).

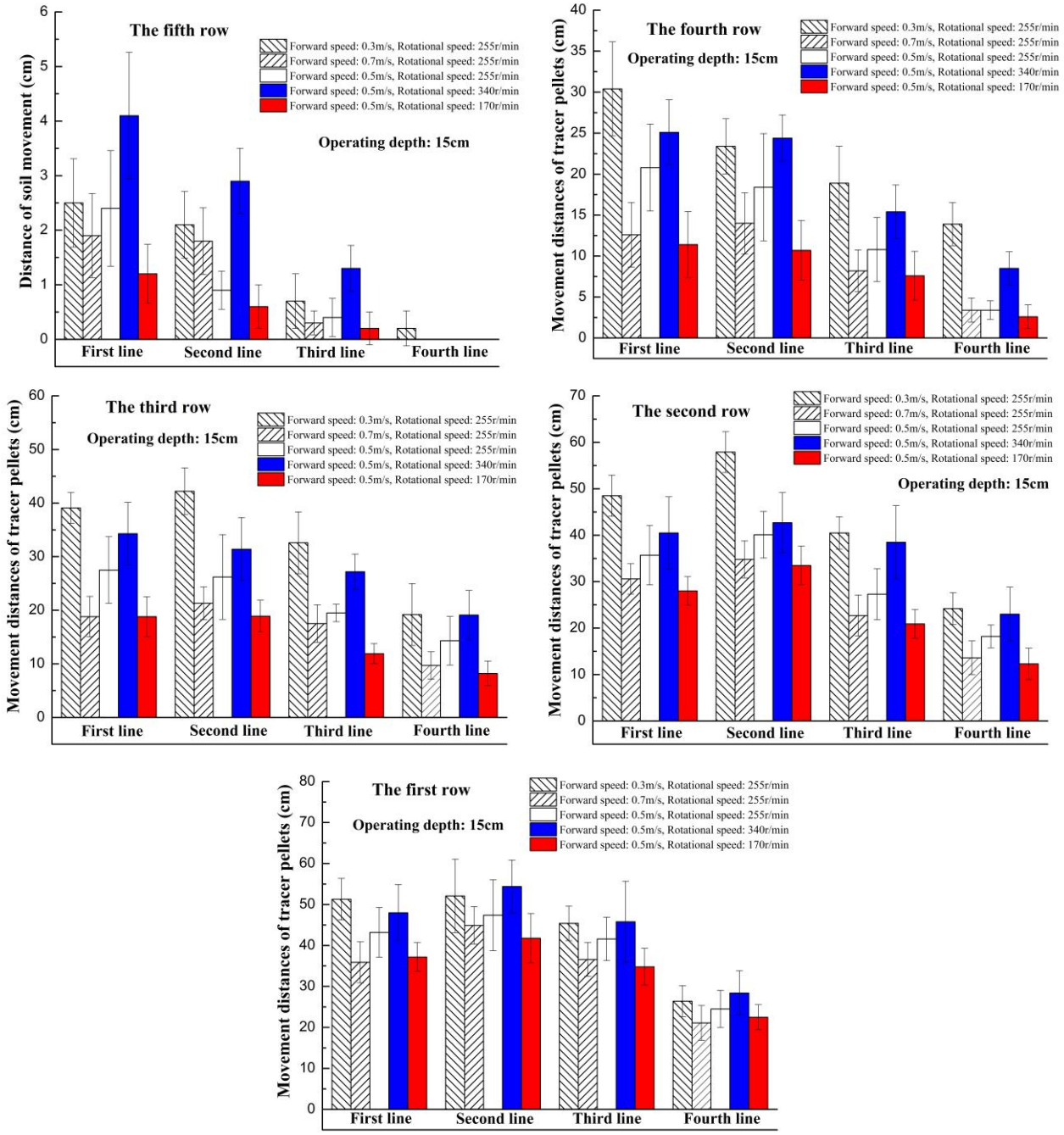

Fig. 11 - Soil movement pattern at different forward speeds and blade rotational speeds

At an operating depth of 15 cm and a forward speed of 0.5 m/s, the movement distance of the tracer pellets in all rows and lines increased as the blade rotational speed increased. This indicates that the soil movement distance increased as the blade rotational speed increased in the normal range. At a blade rotational speed of 340 rpm, the movement distance of the second line in the first row of tracer pellets was the greatest (54.4 cm).

Overall soil movement pattern and its relationship with power consumption

Table 2 summarises the tracer movement pattern at all positions and its relationship with power consumption. Under all the testing conditions, the tracer movement distance in the travel direction accounted for 55–64% of the overall tracer movement distance; along the width, it accounted for 30–37% and along the depth for 5–11%. This indicates that, under all the testing conditions, the soil movement distance in the travel direction accounted for more than half of the overall soil movement distance, followed by the width and depth directions.

For a constant operating depth (15 cm) and blade rotational speed (255 rpm), at a forward speed of 0.5 m/s, the proportions of tracer movement distance in the width and depth directions to the overall tracer movement peaked, whereas the proportion of the tracer movement distance in the travel direction minimised. At a forward speed of 0.3 m/s, the proportions of the tracer movement distance in the width and depth directions to the overall tracer movement were minimised, whereas the proportion of the tracer movement distance in the travel direction peaked. This indicates that the proportions of the soil movement distance in the width depth direction to the overall soil movement distance peaked at a forward speed of 0.5 m/s, whereas the proportion of the soil movement distance in the travel direction peaked at a forward speed of 0.3 m/s.

For a constant operating depth (15 cm) and forward speed (0.5 m/s), at a blade rotational speed of 255 rpm, the proportions of the tracer movement distances along the width and depth directions peaked, whereas the proportions of the tracer movement in the travel direction were minimised. At a blade rotational speed of 340 rpm, the proportions of the tracer movement distances in the width and depth directions were minimised, whereas the proportion of the tracer movement in the travel direction peaked. This indicates that the proportions of the soil movement distance in terms of width and depth to the overall soil movement distance peaked at a blade rotation speed of 255 rpm, whereas the proportion of the soil movement distance in the travel direction peaked at a blade rotation speed of 340 rpm.

Table 2

Overall tracer movement pattern and power consumption

Operating conditions	Overall soil movement distance [cm]	Proportions of soil movement distances in the travel, width, and depth direction to the overall soil movement [%]	Instantaneous torque [N ▪m]	Instantaneous power [kW]	Total power consumption [kW]
Operating depth: 5 cm, Rotational speed: 255 r/min, Forward speed: 0.5 m/s	360.9	33.60, 56.92, 9.48	8.7813	0.234	1.233
Operating depth: 10 cm, Rotational speed: 255 r/min, Forward speed: 0.5 m/s	460.7	33.63, 55.67, 10.70	15.0369	0.402	2.280
Operating depth: 15 cm, Rotational speed: 255 r/min, Forward speed: 0.5 m/s	422.6	36.13, 56.69, 7.18	26.3127	0.703	3.538
Operating depth: 20 cm, Rotational speed: 255 r/min, Forward speed: 0.5 m/s	415.4	33.48, 60.36, 6.16	47.3212	1.264	6.677
Forward speed: 0.3 m/s, Operating depth: 15 cm, Rotational speed: 255 r/min	571.5	33.50, 60.68, 5.82	22.8753	0.611	5.116
Forward speed: 0.7 m/s, Operating depth: 15 cm, Rotational speed: 255 r/min	349.7	31.04, 63.58, 5.38	38.4716	1.027	3.505
Rotational speed: 170 r/min, Operating depth: 15 cm, Forward speed: 0.5 m/s	323.1	35.82, 58.48, 5.70	33.9634	0.605	3.461
Rotational speed: 340 r/min, Operating depth: 15 cm, Forward speed: 0.5 m/s	515.0	30.88, 63.98, 5.14	28.8791	1.028	4.385

With the forward speed (0.5 m/s) and blade rotational speed (225 rpm) constant, the overall tracer movement distance peaked at 460.7 cm at an operating depth of 10 cm, followed by the movement distances at operating depths of 5, 15, and 20 cm. This indicates that soil movement distance peaked at an operating depth of approximately 10 cm. The instantaneous torque (instantaneous power) and total power consumption of the rotary blade increased with the operating depth. This finding is consistent with those obtained by Zhang et al. (2019) and *Fujii et al. (2015)*. This indicates that the instantaneous torque and total power consumption were positively related to the operating depth; however, they were not related to the soil movement distance.

With the operating depth (15 cm) and blade rotational speed (225 rpm) constant, the overall tracer movement distance decreased as the forward speed increased (0.3, 0.5, and 0.7 m/s). The instantaneous torque exhibited an increasing trend with the forward speed, which agrees with the results obtained by *Ahmadi (2017*). This indicates that the instantaneous torque is positively related to the forward speed; however, it is negatively related to the soil movement distance. The total power consumption exhibited a decreasing trend with the forward speed, which is consistent with the results obtained by *Salokhe et al. (2001)*. This indicates that the total power consumption was negatively related to the forward speed; however, it was positively related to the soil movement distance.

With the operating depth (15 cm) and forward speed (0.5 m/s) constant, the overall tracer movement distance increased with the blade rotational speed (170, 255, and 340 rpm). The instantaneous torque was the largest at a blade rotational speed of 170 rpm and was the smallest at a blade rotational speed of 255 rpm, which is consistent with the results obtained by *Gupta* and *Pandey (1996)* and *Matin et al. (2015)* that is, instantaneous torque first decreased then increased. This indicates that the instantaneous torque was not related to the blade rotational speed and soil movement distance. The total power consumption exhibited an increasing trend with the blade rotational speed, which was consistent with the results obtained by Tiwari and *Gite (2006)*. This indicates that the total power consumption was positively related to the blade rotational speed and soil movement distance.

When other operating conditions were held constant, the total power consumption peaked at 6.677 kW at an operating depth of 20 cm and reached a minimum at 1.233 kW at an operating depth of 5 cm. With other operating conditions constant, the total power consumption peaked at 6.677 kW for a forward speed of 0.3 m/s and reached a minimum at 3.505 kW for a forward speed of 0.7 m/s. With other operating conditions constant, the total power consumption peaked at 4.385 kW at a blade rotational speed of 340 rpm and reached a minimum at 3.467 kW at a forward rotational speed of 170 rpm (Table 2).

Based on the investigations on soil movement, changes in the relationship between the operating conditions and power consumption of the rotary blade during furrowing were obtained. Although *Jumin et al. (2014)* and *Thakur and Godwin (1989)* performed similar studies, they only investigated the relationship between operating conditions and power consumption of the rotor blade. As the soil movement is essence that the operating conditions effect the furrowing power consumption. The study researched the correlation soil movement between furrowing power consumption further and could apply to analysing the furrowing power consumption of rotary blade based on soil movement.

CONCLUSIONS

Rotary blades fixed to small handheld furrow openers for preparing small field patches involve soil throwing/movement and energy consumption. This study investigated the relationship between soil movement and power consumption and that between soil movement and operating conditions of such a blade. We draw the following conclusions:

1) The soil movement distance at or closer to the centre of action of the rotary blade was larger than that farther away.

2) Under all testing conditions, the proportion of the soil movement distance in the travel direction to the overall soil movement distance was the largest, with the value larger than 50%, followed by that in the depth direction and then that in the width direction.

3) The soil movement distance of the soil layers with depths of 0–5 cm was the largest at all operating depths. Moreover, soil movement distance decreased as the soil layer depth increased.

4) Generally, soil movement distance increased as the forward speed decreased in the normal range. The soil movement distance increased with the blade rotational speed in the normal range.

5) For constant forward and blade rotational speeds, the instantaneous torque and total power consumption were positively related to the operating depth, however, not related to the soil movement distance.

For constant operating depth and blade rotational speed, the instantaneous torque was positively related to the forward speed, however, negatively related to the soil movement distance; the total power consumption was negatively related to the forward speed, however, positively related to the soil movement distance. With the operating depth and forward speed constant, the instantaneous torque was not related to the blade rotational speed and soil movement distance; the total power consumption was positively related to blade rotational speed and soil movement distance.

Based on the results, it was concluded that by decreasing the operating depth and blade rotational speed and increasing forward speed, the power consumption of the unit working length can be reduced.

ACKNOWLEDGEMENT

This research was supported by the Anhui Province Natural Science Foundation (No: 2008085QE270). The authors wish to thank Mr. Cai Lianhe for his support in adjusting the test platform.

REFERENCES

[1] Ahmadi I., (2017), A torque calculator for rotary tiller using the laws of classical mechanics. *Soil Tillage Res*. 165, 137-143.

[2] Ahmadi I., (2017), A torque calculator for rotary tiller using the laws of classical mechanics, Soil and Tillage Research, vol. 165, ISSN: 0167-1987, pp. 137–143.

[3] Ani O.A., Uzoejinwa B.B., Ezeama A.O., Onwualu P.A., Ugwu S.N., Ohagwu C.J., (2018), Overview of soil-machine interaction studies in soil bins. *Soil and Tillage Research*, vol. 175, ISSN: 0167-1987, pp. 13–27.

[4] Asl J.H., Singh S., (2009), Optimization and evaluation of rotary tiller blades: Computer solution of mathematical relations, *Soil and Tillage Research*, vol. 106, no. 1, ISSN: 0167-1987, pp. 1–7.

[5] Chertkiattipol S., Niyamapa T., (2010), Variations of torque and specific tilling energy for different rotary blades. I*nternational Agricultural Engineering Journal*, vol. 19 no. 3, ISSN: 0858-2114, pp. 1–14.

[6] Fajardo A.L., Suministrado D.C., Peralta E.K., Bato P.M., Paningbatan E.P., (2014), Force and puddling characteristics of the tilling wheel of float-assisted tillers at different lug angle and shaft speed, *Soil and Tillage Research*, vol 140, ISSN: 0167-1987, pp. 118–125.

[7] Fujii T., Hasegawa H., Ohyama T., Sinegovskaya V.T., (2015), Evaluation of tillage efficiency and power requirements for a deep-placement fertilizer applicator with reverse rotational rotary, *Russian Agricultural Sciences,* vol. 41, no. 6, ISSN: 1068-3674, pp. 498 –503.

[8] Grayling K.M., Young S.D., Roberts C.J., De Heer M.I., Shirley I.M., Sturrock C.J., Mooney S.J., (2018). The application of x-ray micro computed tomography imaging for tracing particle movement in soil. *Geoderma*, vol. 321, ISSN: 0016-7061, pp. 8-14.

[9] Gupta J.P., Pandey K.P., (1996), Performance of rotary tiller tines under wetland condition. Agricultural Mechanization in Asia, Africa and Latin America, vol.27, no.1, pp.16–20.

[10] Haas J., Fenner P.T., Schack-Kirchner H., Lang F., (2018.), Quantifying soil movement by forest vehicles with corpuscular metal tracers, *Soil and Tillage Research*, vol. 181, pp. 19–28.

[11] Harrison H.P., (1978), Design of vertical rotary tiller blades for reforestation*. Transactions of the ASAE,* vol. 21, no. 6, ISSN: 0001-2351, pp. 1029–1033.

[12] He C., You Y., Wang D., Wang G., Lu D., Kaji J.M.T., (2016), The effect of tine geometry during vertical movement on soil penetration resistance using finite element analysis, *Computers and* E*lectronics in Agriculture,* 130, ISSN: 0168-1699, pp. 97–108.

[13] Zhang J, He X., Xia J., Zhang S, Zhai J., Gui P., Zhang B., (2014), Design and field experiment of power consumption measurement system for high stubble returning and tillage machine, T*ransactions of the Chinese Society of Agricultural Engineering*, vol. 30, no. 18, ISSN: 1002-6819, pp. 38–46.

[14] Kataoka T., Shibusawa S., (2002), Soil-blade dynamics in reverse-rotational rotary tillage, J*ournal of Terramechanics*, vol. 39, no. 2, ISSN: 0022-4898, pp. 95–113.

[15] Lee K.S., Park S.H., Park W.Y., Lee C.S., (2003), Strip tillage characteristics of rotary tiller blades for use in a dryland direct rice seeder, *Soil and Tillage Research*, vol. 71, no. 1, pp. 25–32.

[16] Li S., Chen X., Chen W., Zhu S., Li Y., Yang L., Xie S., Yang M., (2018), Soil-cutting simulation and parameter optimization of handheld tiller's rotary blade by smoothed particle hydrodynamics modelling and Taguchi method, *Journal of Cleaner Production*, vol. 179, ISSN: 0959-6526, pp. 55–62.

[17] Matin M.A., Fielke J.M., Desbiolles J.M.A., (2015), Torque and energy characteristics for strip-tillage cultivation when cutting furrows using three designs of rotary blade. *Biosystems Engineering,* vol. 129, ISSN: 1537-5110, pp. 329–340.

[18] Mollazade K., Ahmadi H., Alimardani R., (2009), Optimal design of rotary tiller's rotor and width proportionate to tractor power using energy method, *International Journal of Agricultural and Biological Engineering,* vol. 2, no. 2, ISSN: 1934-6344, pp. 1–7.

[19] Qin K., Ding W., Ahmad F., Fang Z., (2018), Design and experimental validation of sliding knife notch-type disc opener for a no-till combine harvester cum seed drill, *International Journal of Agricultural and Biological Engineering*, vol. 11, no. 4, ISSN: 1934-6344, pp. 76–85.

[20] Rahman S., Chen Y., Lobb D., (2005), Soil movement resulting from sweep type liquid manure injection tools, *Biosystems Engineering*, vol. 91, no. 3, ISSN: 1537-5110, pp. 379–392.

[21] Salokhe V. M., Ramalingam N., (2001), Effects of direction of rotation of a rotary tiller on properties of Bangkok clay soil, *Soil and Tillage Research*, 63(1-2), ISSN: 0167-1987, pp. 65-74.

[22] Salokhe V. M., Ramalingam N., (2002), Effect of rotation direction of a rotary tiller on draft and power requirements in a Bangkok clay soil, *Journal of Terramechanics,* vol. 39, no. 4, pp. 195–205.

[23] Shibusawa S., (1993), Reverse-rotational rotary tiller for reduced power requirement in deep tillage, *Journal of Terramechanics*, vol. 30, no. 3, ISSN: 0022-4898, pp. 205–217.

[24] Solhjou A., Fielke J.M., Desbiolles J.M.A., (2012), Soil translocation by narrow openers with various rake angles, *Biosystems Engineering,* vol. 112 no. 1, ISSN: 1537-5110, pp. 65–73.

[25] Thakur T.C., Godwin R.J., (1989), The present state of force prediction models for rotary powered tillage tools, Journal of Terramechanics, vol. 26, no. 2, ISSN: 0022-4898, pp. 121–138.

[26] Tiwari P.S., Gite L.P., (2006), Evaluation of work-rest schedules during operation of a rotary power tiller. *International Journal of Industrial Ergonomics*, vol. 36, no. 3, ISSN: 0169-8141, pp. 203–210.

[27] Ucgul M., Saunders C., Fielke J.M., (2017), Discrete element modelling of tillage forces and soil movement of a one-third scale mouldboard plough. *Biosystems Engineering,* vol. 155, pp. 44–54.

[28] Ucgul M., Saunders C., Li P., Lee S.H., Desbiolles J.M.A., (2018), Analysing the mixing performance of a rotary spader using digital image processing and discrete element modelling (DEM), *Computers and Electronics in Agriculture*, vol. 151, ISSN: 0168-1699, pp. 1–10.

[29] Viktor M., Munkholm L.J., Ying C., Tavs N., (2018), Modelling approach for soil displacement in tillage using discrete element method, *Soil and Tillage Research,* vol. 183, pp. 60–71.

[30] Yang M.J., Niu P., Peng B., Yang L., Li Y.W., Chen X.B., Peng Z.M., (2015), Soil-cutting performance analysis of a handheld tiller's rotavator by finite element method (fem). *INMATEH – Agricultural Engineering*, vol. 47, no. 3, ISSN: 2068-4215, pp.13–20.

[31] Zhang G.S., Zhang Z.Q., Xiao M.H., Bartos P., Bohata A., (2019), Soil-cutting simulation and parameter optimization of rotary blade's three-axis resistances by response surface method. *Computers and Electronics in Agriculture,* vol. 164, ISSN: 0168-1699, 104902.